Band Structure and Terahertz Optical Conductivity of Transition Metal Oxides: Theory and Application to CaRuO_{3}

Hung T. Dang, Jernej Mravlje, Antoine Georges, and Andrew J. Millis

Phys. Rev. Lett. **115**, 107003 — Published 3 September 2015

DOI: 10.1103/PhysRevLett.115.107003

Band structure and the THz scale optical conductivity of transition metal oxides: theory and application to $CaRuO_3$

Hung T. Dang,[1] Jernej Mravlje,[2] Antoine Georges,[3,4,5] and Andrew J. Millis[6]

[1] *Institute for Theoretical Solid State Physics, JARA-FIT and JARA-HPC, RWTH Aachen University, 52056 Aachen, Germany*
[2] *Jožef Stefan Institute, Jamova 39, Ljubljana, Slovenia*
[3] *Collège de France, 11 place Marcelin Berthelot, 75005 Paris, France*
[4] *Centre de Physique Théorique, Ecole Polytechnique, CNRS, 91128 Palaiseau Cedex, France*
[5] *DQMP, Université de Genève, 24 quai Ernest-Ansermet, 1211 Genève 4, Switzerland*
[6] *Department of Physics, Columbia University, New York, New York 10027, USA*

(Dated: August 10, 2015)

Density functional plus dynamical mean field calculations are used to show that in transition metal oxides, rotational and tilting ($GdFeO_3$-type) distortions of the ideal cubic perovskite structure produce a multiplicity of low energy optical transitions which affect the conductivity down to frequencies of the order of one or two millivolts (terahertz regime), mimicking non-Fermi-liquid effects even in systems with a strictly Fermi liquid self-energy. For $CaRuO_3$, a material whose measured electromagnetic response in the terahertz frequency regime has been interpreted as evidence for non-Fermi-liquid physics, the combination of these band structure effects and a renormalized Fermi liquid self-energy accounts for the low frequency optical response which had previously been regarded as a signature of exotic physics. Signatures of deviations from Fermi liquid behavior at higher frequencies (~ 100 meV) are discussed.

Fermi liquid theory provides the canonical picture of metals; observation of deviations from Fermi liquid behavior is thus of intense interest as a potential indication of novel physics. The defining feature of a Fermi liquid is the existence of electron-like quasiparticles whose low temperature and frequency properties are characterized by an effective mass that is independent of frequency and a scattering rate that is parametrically smaller than frequency or temperature (typically varying as ω^2 or T^2). The perovskite ruthenate $CaRuO_3$ has been the subject of considerable attention in this context because its frequency dependent conductivity has been reported [1, 2] to vary as a power of frequency with exponent less than unity. The anomalous dependence extends to very low frequencies of the order of 1 THz ($\sim$ 4 meV) [2], and has been interpreted as indicating a breakdown of Fermi liquid physics in this material. Similar interpretations have been given of optical data in $SrRuO_3$ [3]. On the other hand, recent *dc* transport measurements in $CaRuO_3$ found quantum oscillations and a quadratic temperature dependence of the resistivity [4] below 1.5 K – characteristic of a Fermi liquid. The link between the frequency-dependent and *dc* transport measurements has not been established and a model accounting for the optical conductivity is not known.

In this paper we present density functional (DFT) plus dynamical mean field (DMFT) calculations which indicate that band structure effects associated with octahedral rotations of the ideal perovskite crystal structure produce optically active interband transitions that contribute to the conductivity on scales as low as 1 THz ($\sim$ meV) and can mimic non-Fermi-liquid physics. As an application we show that the observed THz conductivity of $CaRuO_3$ is consistent with Fermi-liquid-like quasiparticles and quantify the departures from Fermi liquid physics that occur at higher scales.

The standard arguments relating optical conductivity $\sigma(\Omega)$ and electron self-energy $\Sigma(\omega)$ may conveniently be framed in terms of an approximation due to Allen [5–7]:

$$\sigma(\Omega) \propto \frac{i}{\Omega}\int d\omega \frac{f(\omega)-f(\omega+\Omega)}{\Omega-\Sigma(\Omega+\omega)+\Sigma^{\star}(\omega)}. \qquad (1)$$

Here f is the Fermi function and the * denotes complex conjugation. Eq. (1) is expected to be reasonable when interband transitions are neglected.

In a simple Drude metal, $\Sigma = -i/(2\tau)$ with 2τ the time between scatterings of electrons off of impurities. Use of this self-energy in Eq. (1) yields the familiar Drude conductivity $\sigma(\Omega) \propto \tau/(1-i\Omega\tau)$. Use of the Fermi liquid form $\Sigma(\omega) \propto (1-Z^{-1})\omega - i\Omega_0^{-1}\left(\omega^2+\pi^2T^2\right)$ yields a conductivity with a characteristic scaling form [8], see also Refs. [9, 10], that we will refer to as the single-band Fermi liquid (SBFL) conductivity. If the self-energy takes the non-Fermi-liquid form $\Sigma(\omega) \sim \omega^x$ with $x < 1$ one has $|\Sigma(\omega)| > |\omega|$ at low frequency, so that the term proportional to Ω in the denominator of the argument of the integral in Eq. (1) may be neglected. A scaling analysis of Eq. (1) then shows that for small Ω, $\sigma \sim \Omega^{-x}$, with the divergence cut off by temperature.

We compare expectations based on Eq. (1) to realistic calculations of the frequency dependent conductivity of $CaRuO_3$. This material crystallizes in a $GdFeO_3$-distorted version of the ideal cubic perovskite structure. In the latter, there are three near-Fermi-surface bands derived from the three t_{2g} states. The $GdFeO_3$-distorted structure has four Ru ions in the unit cell, leading to

12 t_{2g}-derived near-Fermi-surface bands. The t_{2g}-derived bands are the eigenvalues of a Hamiltonian matrix $H_0(\mathbf{k})$ with $\mathbf{k}$ a wavevector in the first Brillouin zone. $H_0(\mathbf{k})$ is obtained by using maximally localized Wannier function (MLWF) [11, 12] techniques to project the Kohn-Sham Hamiltonian found from a spin-unpolarized DFT band calculation onto the near-Fermi-surface states. The effects of electron-electron interactions are encoded in the self-energy $\Sigma(\mathbf{k},\omega)$, also a matrix, which we compute by applying single-site DMFT to the $H_0(\mathbf{k})$ corresponding to the experimental structure of $CaRuO_3$ with standard Slater-Kanamori interactions parametrized by $U = 2.3$ eV and $J = 0.4$ eV (see Supplementary Material, which includes Refs. 11–25, for details of DFT and DMFT calculations). Electron propagation in the t_{2g}-derived bands is thus described by the $N \times N$ matrix Green function ($N = 3$ for the cubic structure and 12 for the experimental one)

$$\mathbf{G}(k,\omega) = [\omega + \mu - H_0(\mathbf{k}) - \Sigma(\omega)]^{-1}\,. \qquad (2)$$

For the situations we consider there are no vertex corrections to the current operator in the single-site dynamical mean field approximation, essentially because no on-site optical transitions are allowed (see Supplementary Material for a more detailed discussion and also Ref. 26 for the single-band case) so the conductivity becomes

$$\sigma(\Omega) = \int \frac{d\omega}{\pi} \frac{f(\omega) - f(\omega+\Omega)}{\Omega} \times \mathrm{Tr}\left[J_{\mathbf{k}} \mathrm{Im}G(\mathbf{k},\omega+\Omega) J_{\mathbf{k}} \mathrm{Im}G(\mathbf{k},\omega)\right]. \qquad (3)$$

The matrix current operator $J_{\mathbf{k}}$ is derived in a standard way from $H_0(\mathbf{k})$ (note that in systems with more than one atom per unit cell, care must be taken to use a basis in which each atom acquires the Peierls phase appropriate to its physical position within the unit cell [27, 28]). The trace is over momentum and band indices. In our calculations, the four-dimensional integral (in frequency and momentum space) is performed using Gaussian quadrature with 60 points in each direction. The Allen formula [Eq. (1)] may be derived from Eq. (3) if the matrices are diagonal (no interband transitions) and when the transport function (i.e. the density of states weighted by current matrix elements) depends weakly on energy.

The main panel of Fig. 1 presents the normalized conductivity calculated using Eq. (3) with $H_0(\mathbf{k})$, $J_{\mathbf{k}}$ and Σ appropriate to the experimental structure of $CaRuO_3$. The conductivity in the mid-infrared regime (5 meV $\lesssim \Omega \lesssim$ 250 meV) appears to vary as a power law $\sim \omega^{-x}$ with x in the range $0.4-0.6$, similar to the power law reported experimentally [1]. The lower inset compares the calculated conductivity to recent measurements [4], which come from samples with significantly lower impurity scattering than samples studied earlier [2]. The quantitative correspondence between calculation and data is good.

Also shown in Fig. 1 are the conductivities obtained from Eq. (3) using the $H_0(\mathbf{k})$ and $J_{\mathbf{k}}$ corresponding to

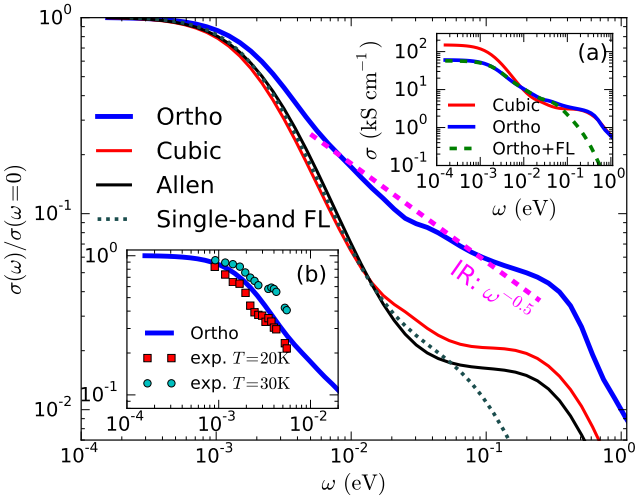

FIG. 1. (Color online) Main panel: optical conductivity (normalized to its zero frequency value). Heavy solid line (blue online): conductivity computed from DFT+DMFT at $T = 30$ K for the orthorhombic experimental structure. The dashed straight line is a guide to the eye indicating the power-law behaviour $\sim \omega^{-0.5}$, corresponding to the experimentally reported mid-IR frequency dependence [1]. Also displayed are the conductivities computed for hypothetical cubic structure (intermediate weight line, red online) and from the Allen formula (light line, black online), using the same DMFT self-energy as used in the experimental structure calculation. Finally, the dotted line presents the 'SBFL' result obtained by using a Fermi liquid self-energy in the Allen formula. Inset (a): optical conductivity calculated using DMFT self-energy for experimental structure and cubic structure compared to a calculation (dashed lines) for the experimental structure but with a Fermi-liquid self-energy [Eq. (4)]. Inset (b): experimental data of Ref. 4 in the THz range along with the DMFT calculation for the realistic structure.

the ideal cubic structure (while keeping the same self-energies as for the real structure) and by using the Allen formula [Eq. (1)] again for the same self-energies. (The Allen formula results are obtained as an equally weighted sum over three terms, one for each diagonal entry in the self-energy matrix). In the THz and sub-THz regime ($\omega \sim 1-10$ meV) the cubic/Allen results exhibit a much more rapid rolloff from the *dc* plateau than does the experimental structure conductivity, while in the mid-IR ($\omega \sim 100$ meV) regime the cubic/Allen results exhibit an approximate plateau if the DMFT self-energy is used.

As the self-energies used in the cubic and orthorhombic calculations are exactly the same, the difference between the results is not a self-energy effect and does not correspond to non-Fermi-liquid physics. To probe the effect of the self-energy, we also display in the main panel the SBFL result (with parameters Z, Ω_0 determined from a fit to the DMFT self-energy in Fig. 3), and in the inset (a) the conductivity obtained when using a Fermi-liquid self-energy and the realistic orthorhombic structure. We

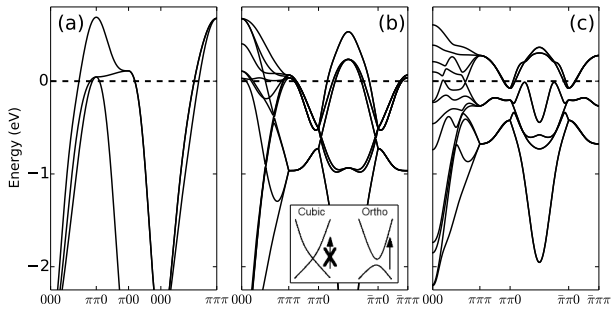

FIG. 2. Band structure computed for (a): the ideal cubic perovskite form of $CaRuO_3$ plotted along high symmetry directions in the cubic perovskite Brillouin zone. (b): the ideal cubic structure folded back into the Brillouin zone of the experimental orthorhombic structure. (c): the experimental orthorhombic structure, along high symmetry directions of the orthorhombic Brillouin zone. All three panels show the frontier t_{2g}-antibonding bands produced by MLWF fitting of the DFT (GGA) band structure. Inset: Optical transitions across minigaps which are forbidden in the cubic structure are activated in the distorted structure.

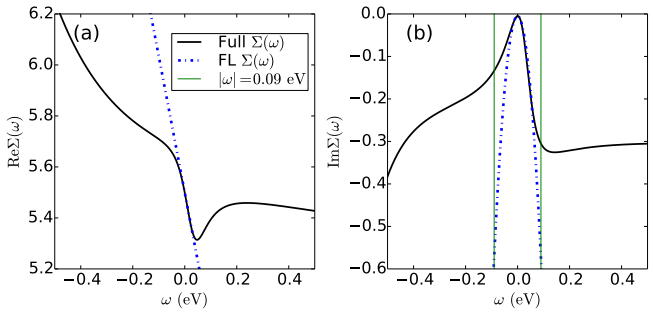

FIG. 3. (Color online) (a): Real part of the self-energy for one of the three orbitals (solid line). Dashed-dotted line: linear low-frequency fit to the real part of Eq. (4) with slope $1 - Z^{-1} \equiv d\Sigma/d\omega = -5.3$. (b): Imaginary part of self-energy of the same orbital (solid line). Dashed-dotted line: low-energy Fermi liquid fit to the imaginary part of Eq. (4) with $\Omega_0 \simeq 14$ meV and temperature $T = 0.0025$ meV ≈ 30 K. Vertical lines: boundary of the Fermi liquid region ($\omega = 0.09$ eV).

see that the choice of self-energy hardly influences the low frequency result; it is only at frequencies higher than ~ 50 meV that the choice of self-energy significantly influences the calculation.

The key approximation of both the Allen and SBFL formula is the neglect of interband transitions. The difference between these approximations and the calculation for the experimental structure thus arises from optically active interband transitions, which are seen to affect the conductivity down to scales as low as 1 THz. To explicate the origin of these transitions we present in Fig. 2 our calculated band structures. The left panel shows the near-Fermi-surface bands found for the ideal cubic structure. Direct interband transitions between the three bands are possible in principle; however the different orbital symmetry of the different bands means that the matrix elements are small, especially in the lower frequency regime, so that the cubic and Allen results are similar. At higher energies, interband transitions have some effect in the cubic structure as well.

The middle panel shows the bands of the cubic structure, folded into the Brillouin zone of the experimental structure. The backfolding creates the possibility of many low-lying interband transitions, but in the cubic structure these transitions are not optically active as they do not correspond to zero-momentum transfer. The right panel shows the band structure obtained for the experimental structure. The octahedral rotations reduce the overlap between states on different sites, causing a band narrowing from 3.6 eV to 2.6 eV visible for example in the energies near the Γ point and flattening the dispersion in the near-Fermi-surface region. The zero frequency conductivity of the orthorhombic case is thus smaller (by a factor of ~ 3) than the cubic result (see inset Fig. 1). The rotations also allow matrix elements between nearby states, opening additional minigaps where the cubic bands cross, further flattening the bands at the Fermi level and, crucially, activating optical matrix elements between the backfolded bands. Starting at $\omega \sim 1$ meV, these become important, changing the functional form of the conductivity. At high frequencies the experimental and cubic structure conductivities become very similar, as the small gaps are unimportant.

To study the nature of the non-Fermi-liquid effects in the conductivity of $CaRuO_3$ we present in Fig. 3 a plot of the real and imaginary parts of the self-energy calculated for one of the three t_{2g} orbitals (the self-energies associated with the other two are similar). Also shown is a fit of the self-energy to the functional form

$$\Sigma_{FL}(\omega, T) = \left(1 - Z^{-1}\right)\omega - i\,\Omega_0^{-1}\left[\omega^2 + b\,(\pi T)^2\right]. \quad (4)$$

Here Z is a dimensionless constant giving the mass renormalization $m^\star/m \equiv Z^{-1}$, T is the temperature and the characteristic energy Ω_0 sets the scale of the scattering rate. The parameter $b = 1$ (Fermi liquid) for the plotted orbital but about $2 - 3$ for the other two perhaps because the coherence temperature is not quite reached. From Fig. 3 we see that at very low frequencies $|\omega| \lesssim 20$ meV the self-energy approximately takes the Fermi liquid form, but for larger frequencies $\omega \gtrsim 40$ meV pronounced ($\gtrsim 50\%$) deviations occur. On the positive frequency (electron addition) side the imaginary part of the self-energy saturates for $\omega \gtrsim 0.1$ eV and the real part loses most of its frequency dependence. On the negative frequency (electron removal) side the imaginary part of the self-energy increases (although not as rapidly as the Fermi liquid ω^2) and exhibits a large peak (not shown) at $\omega \sim -1$ eV. The low frequency at which deviations from Fermi liquid behavior occur is characteristic of multiorbital systems with sizeable Hund's coupling [29].

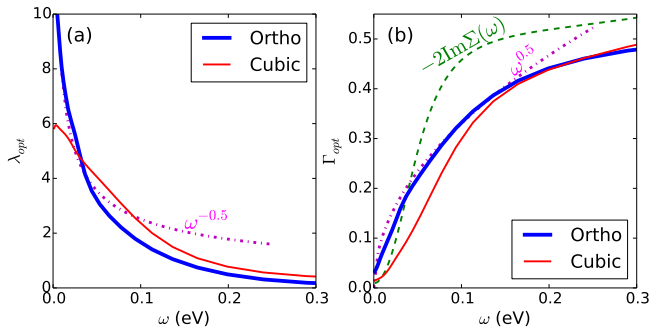

FIG. 4. (Color online) Optical mass (a) and scattering rate (b) obtained via Eq. (5) for different cases considered in this paper and compared to quasiparticle mass (~ 6.7 as calculated from the slope of $\mathrm{Im}\Sigma(i\omega_n)$) and the imaginary part of the single particle self-energy (dashed curve - green online). Dotted curves (magenta online) indicate $\omega^{\pm 0.5}$ behavior.

At very low frequency ($\lesssim 7.5$ meV), $\omega < \pi T$ the scattering rate is in effect constant so the cubic and Allen-formula conductivities in Fig. 1 are indeed well described by a Drude form with frequency independent scattering rate $\Gamma_{Drude} = 2Z(\pi T)^2/\Omega_0 \approx 1.4$ meV. However, in the orthorhombic structure interband transitions cause the conductivity to decay much less rapidly than expected from the Drude formula at frequencies $\gtrsim 1$ meV.

Suppose now that the self-energy was well described by the Fermi liquid form even at frequencies higher than ~ 20 meV. Inspection of the upper inset of Fig. 1 shows that for $\Omega \gtrsim 100$ meV the corresponding conductivity becomes much smaller than either the cubic or the experimental system conductivity. (One sees this from the behavior of the SBFL curve in the main panel of Fig. 1, but it can also be derived directly (see Supplementary Material) by inserting Eq. (4) into Eq. (1), setting temperature $T = 0$ and scaling the internal integration variable by the external frequency Ω to yield $\sigma_{FL}(\Omega) \propto Z \int_{-1}^{0} dx \left(-i\Omega + Z\Omega_0^{-1}\Omega^2(1+2x+2x^2)\right)^{-1}$. The real part of this expression has an approximately Lorentzian Drude-like decay with decay constant $\Omega_0/Z \approx 80$ meV, which describes well the high-frequency behavior of the Fermi liquid results.) The slower decay of the actual conductivity is a signature of deviations from Fermi-liquid physics. It results in particular from the saturation of the scattering rate and strong deviation of $\mathrm{Re}\Sigma(\omega)$ [20] from the low frequency linear behavior apparent on Fig. 3. In this non-Fermi liquid higher-frequency regime, the similarity of the conductivities for the cubic and experimental structure conductivities shows that here band structure effects are of less importance, implying that information about the self-energy may be extracted from the conductivity.

Formally inverting Eq. (1) or Eq. (3) to obtain self-energies from measured conductivities is an ill-posed and essentially not solvable inversion problem. However the widely used 'memory function' method [30] provides considerable insight. The typical procedure is to express the complex conductivity $\tilde{\sigma}$ in terms of an optical mass enhancement λ_{opt} and scattering rate Γ_{opt} defined as

$$\tilde{\sigma} = \frac{K}{-i\omega\left(1+\lambda_{opt}(\omega)\right)+\Gamma_{opt}(\omega)}. \qquad (5)$$

The objects λ_{opt} and Γ_{opt} are often interpreted as mass enhancement and scattering rate respectively and assumed to provide information about the electron self-energy. Their frequency dependence is determined by the frequency dependence of the complex conductivity while the overall magnitude is determined by the constant $K = 2/\pi \int_0^\infty \mathrm{Re}\tilde{\sigma}(\omega)d\omega$. In the two panels of Fig. 4 we present the λ_{opt} and Γ_{opt} determined from our calculations, using the directly computed sum rule values $K_{cubic} = 0.165$ eV and $K_{ortho} = 0.153$ eV (computed for the orthorhombic b direction).

For the cubic and Allen formula cases, where interband transitions are not important, the scattering rate found from the memory function is in reasonable agreement with a particle-hole average of imaginary part of the self-energy. The scattering rate magnitude is correctly estimated and the low frequency ω^2 behavior is clear. The low frequency limit of the mass corresponds precisely to the quasiparticle mass enhancement and the decrease of mass at higher frequency reflects the flattening of the $\mathrm{Re}\Sigma$ curve [9].

For calculations performed with the experimental structure the situation is different: at low frequencies the inferred scattering rate is too large by a factor $\gtrsim 2-4$ and has the wrong concavity. In fact the inferred scattering rate is roughly consistent with an $\omega^{\frac{1}{2}}$ behavior and similarly over a limited low frequency range the optical mass can be fit as $\omega^{-\frac{1}{2}}$. This suggests that caution is warranted in performing a memory function analysis of the low frequency data on $GdFeO_3$-distorted materials. However the reasonable correspondence at higher frequencies ($\omega \gtrsim 100$ meV) between the optical scattering rate and the imaginary part of the self-energy (averaged over positive and negative frequencies) again confirms that in this range the conductivity does give a reasonable estimate of the magnitude and the saturation frequency of the self-energy, and in this sense reveals non-Fermi-liquid behavior of the Hund's metal kind.

In summary, using $CaRuO_3$ as an example we have shown that real materials effects, in particular a multiplicity of optically allowed low-lying transitions arising from band folding due to rotational and tilt distortions, can produce a low frequency conductivity of the form previously associated with non-Fermi-liquid physics. A direct diagnosis of universal Fermi-liquid behaviour from the optical conductivity, along the lines of Ref. 8, only applies when such effects are not important. Our results call for a reexamination of other reports of unusual optical response, for instance in $SrRuO_3$, which has a

ferromagnetic ground state and a smaller orthorhombic distortion, and for which ARPES spectra consistent with Fermi-liquid behavior are observed [31]. It is also important to examine if interband transitions complicate the analysis [32–36] of the ratio of the T^2 and ω^2 terms in the optical scattering rate, which has been argued to be inconsistent with Fermi liquid theory.

H.T.D. acknowledges support from the Deutsche Forschungsgemeinschaft (DFG) within projects FOR 1807 and RTG 1995, as well as the allocation of computing time at Jülich Supercomputing Centre and RWTH Aachen University through JARA-HPC. J.M. acknowledges support of the Slovenian research agency under program P1-0044. A.G. acknowledges a grant from the European Research Council (ERC-319286 QMAC) and the Swiss National Science Foundation (NCCR-MARVEL). A.J.M. acknowledges support from NSF-DMR-1308236.

[1] Y. S. Lee, J. Yu, J. S. Lee, T. W. Noh, T.-H. Gimm, H.-Y. Choi, and C. B. Eom, Phys. Rev. B **66**, 041104 (2002).
[2] S. Kamal, D. M. Kim, C. B. Eom, and J. S. Dodge, Phys. Rev. B **74**, 165115 (2006).
[3] P. Kostic, Y. Okada, N. C. Collins, Z. Schlesinger, J. W. Reiner, L. Klein, A. Kapitulnik, T. H. Geballe, and M. R. Beasley, Phys. Rev. Lett. **81**, 2498 (1998).
[4] M. Schneider, D. Geiger, S. Esser, U. S. Pracht, C. Stingl, Y. Tokiwa, V. Moshnyaga, I. Sheikin, J. Mravlje, M. Scheffler, and P. Gegenwart, Phys. Rev. Lett. **112**, 206403 (2014).
[5] P. B. Allen, Phys. Rev. B **3**, 305 (1971).
[6] P. B. Allen, (2004), arXiv:0407777 [cond-mat.other].
[7] D. N. Basov, R. D. Averitt, D. van der Marel, M. Dressel, and K. Haule, Rev. Mod. Phys. **83**, 471 (2011).
[8] C. Berthod, J. Mravlje, X. Deng, R. Žitko, D. van der Marel, and A. Georges, Phys. Rev. B **87**, 115109 (2013).
[9] D. Stricker, J. Mravlje, C. Berthod, R. Fittipaldi, A. Vecchione, A. Georges, and D. van der Marel, Phys. Rev. Lett. **113**, 087404 (2014).
[10] D. L. Maslov and A. V. Chubukov, Phys. Rev. B **86**, 155137 (2012).
[11] N. Marzari and D. Vanderbilt, Phys. Rev. B **56**, 12847 (1997).
[12] I. Souza, N. Marzari, and D. Vanderbilt, Phys. Rev. B **65**, 035109 (2001).
[13] W. Bensch, H. W. Schmalle, and A. Reller, Solid State Ionics **43**, 171 (1990).
[14] P. Giannozzi, S. Baroni, N. Bonini, M. Calandra, R. Car, C. Cavazzoni, D. Ceresoli, G. L. Chiarotti, M. Cococcioni, I. Dabo, A. Dal Corso, S. de Gironcoli, S. Fabris, G. Fratesi, R. Gebauer, U. Gerstmann, C. Gougoussis, A. Kokalj, M. Lazzeri, L. Martin-Samos, N. Marzari, F. Mauri, R. Mazzarello, S. Paolini, A. Pasquarello, L. Paulatto, C. Sbraccia, S. Scandolo, G. Sclauzero, A. P. Seitsonen, A. Smogunov, P. Umari, and R. M. Wentzcovitch, Journal of Physics: Condensed Matter **21**, 395502 (19pp) (2009).
[15] We used the pseudopotentials Ca.pbe-nsp-van.UPF, Ru.pbe-n-van.UPF and O.pbe-rrkjus.UPF from `www.quantum-espresso.org/pseudopotentials`.
[16] J. P. Perdew, K. Burke, and M. Ernzerhof, Phys. Rev. Lett. **77**, 3865 (1996).
[17] K. Momma and F. Izumi, Journal of Applied Crystallography **44**, 1272 (2011).
[18] A. A. Mostofi, J. R. Yates, Y.-S. Lee, I. Souza, D. Vanderbilt, and N. Marzari, Computer Physics Communications **178**, 685 (2008).
[19] M. Imada, A. Fujimori, and Y. Tokura, Rev. Mod. Phys. **70**, 1039 (1998).
[20] J. Mravlje, M. Aichhorn, T. Miyake, K. Haule, G. Kotliar, and A. Georges, Phys. Rev. Lett. **106**, 096401 (2011).
[21] L. Vaugier, H. Jiang, and S. Biermann, Phys. Rev. B **86**, 165105 (2012).
[22] H. T. Dang, J. Mravlje, A. Georges, and A. J. Millis, Phys. Rev. B **91**, 195149 (2015).
[23] P. Werner, A. Comanac, L. de' Medici, M. Troyer, and A. J. Millis, Phys. Rev. Lett. **97**, 076405 (2006).
[24] O. Parcollet, M. Ferrero, T. Ayral, H. Hafermann, I. Krivenko, L. Messio, and P. Seth, Computer Physics Communications (2015), in press.
[25] H. J. Vidberg and J. Serene, Journal of Low Temperature Physics **29**, 179 (1977).
[26] A. Khurana, Phys. Rev. Lett. **64**, 1990 (1990).
[27] X. Wang, L. de' Medici, and A. J. Millis, Phys. Rev. B **83**, 094501 (2011).
[28] J. M. Tomczak and S. Biermann, Phys. Rev. B **80**, 085117 (2009).
[29] A. Georges, L. d. Medici, and J. Mravlje, Annual Review of Condensed Matter Physics **4**, 137 (2013).
[30] D. N. Basov and T. Timusk, Rev. Mod. Phys. **77**, 721 (2005).
[31] D. E. Shai, C. Adamo, D. W. Shen, C. M. Brooks, J. W. Harter, E. J. Monkman, B. Burganov, D. G. Schlom, and K. M. Shen, Phys. Rev. Lett. **110**, 087004 (2013).
[32] P. E. Sulewski, A. J. Sievers, M. B. Maple, M. S. Torikachvili, J. L. Smith, and Z. Fisk, Phys. Rev. B **38**, 5338 (1988).
[33] T. Katsufuji and Y. Tokura, Phys. Rev. B **60**, 7673 (1999).
[34] J. Yang, J. Hwang, T. Timusk, A. S. Sefat, and J. E. Greedan, Phys. Rev. B **73**, 195125 (2006).
[35] U. Nagel, T. Uleksin, T. Rõõm, R. P. S. M. Lobo, P. Lejay, C. C. Homes, J. S. Hall, A. W. Kinross, S. K. Purdy, T. Munsie, T. J. Williams, G. M. Luke, and T. Timusk, Proc. Natl. Acad. Sci. USA **109**, 19161 (2012).
[36] S. I. Mirzaei, D. Stricker, J. N. Hancock, C. Berthod, A. Georges, E. van Heumen, M. K. Chan, X. Zhao, Y. Li, M. Greven, N. Barišić, and D. van der Marel, Proceedings of the National Academy of Sciences **110**, 5774 (2013).